The Complexity of Functional Connectivity Profiles of the Subgenual Anterior Cingulate Cortex and Dorsal Lateral Prefrontal Cortex in Major Depressive Disorder: a DIRECT Consortium Study

Xiao Chen[1,2,3,4,5], Bin Lu[1,2,3,4], Yu-Wei Wang[1,2,3,4], Xue-Ying Li[1,2,3,4], Zi-Han Wang[1,2,3,4], Hui-Xian Li[1,2,3,4], Yi-Fan Liao[1,2,3,4], Daniel M. Blumberger[5,6], Francisco Xavier Castellanos[7,8], Li-Ping Cao[9], Guan-Mao Chen[10], Jian-Shan Chen[9], Tao Chen[11], Tao-Lin Chen[12,13], Yu-Qi Cheng[14], Zhao-Song Chu[14], Shi-Xian Cui[1,15,16], Xi-Long Cui[17], Zhao-Yu Deng[1,2,3,4], Qi-Yong Gong[12,13], Wen-Bin Guo[17], Can-Can He[18], Zheng-Jia-Yi Hu[1,15,16], Qian Huang[19], Xin-Lei Ji[17], Feng-Nan Jia[20], Li Kuang[19], Bao-Juan Li[21], Feng Li[22], Tao Li[23,24], Tao Lian[1,2,3], Xiao-Yun Liu[25], Yan-Song Liu[20], Zhe-Ning Liu[17], Yi-Cheng Long[17], Jian-Ping Lu[26], Jiang Qiu[27], Xiao-Xiao Shan[17], Tian-Mei Si[28], Peng-Feng Sun[29], Chuan-Yue Wang[22], Hua-Ning Wang[21], Xiang Wang[17], Ying Wang[10], Xiao-Ping Wu[29], Xin-Ran Wu[27], Yan-Kun Wu[28], Chun-Ming Xie[18], Guang-Rong Xie[17], Peng Xie[30,31,32], Xiu-Feng Xu[14], Zhen-Peng Xue[26], Hong Yang[11], Jian Yang[31], Hua Yu[23,24], Yong-Qiang Yu[33,34,35], Min-Lan Yuan[36], Yong-Gui Yuan[25], Yu-Feng Zang[37,38], Ai-Xia Zhang[39], Ke-Rang Zhang[39], Wei Zhang[36], Zi-Jing Zhang[1,2,3], Jing-Ping Zhao[17], Jia-Jia Zhu[33,34,35], Xi-Nian Zuo[40,41], the DIRECT Consortium[#], Chao-Gan Yan[1,2,3,4,15,16]*

[1]CAS Key Laboratory of Behavioral Science, Institute of Psychology, Beijing 100101, China

[2]International Big-Data Center for Depression Research, Chinese Academy of Sciences, Beijing 100101, China

[3]Magnetic Resonance Imaging Research Center, Institute of Psychology, Chinese Academy of Sciences, Beijing 100101, China

[4]Department of Psychology, University of Chinese Academy of Sciences, Beijing 100049, China

[5]Temerty Centre for Therapeutic Brain Intervention, Campbell Family Research Institute, Centre for Addiction and Mental Health, Toronto M6J1H4, Ontario, Canada

[6]Department of Psychiatry, Temerty Faculty of Medicine, University of Toronto, Toronto M5S1A1,

Ontario, Canada

[7]Department of Child and Adolescent Psychiatry, NYU Grossman School of Medicine, New York, NY, USA

[8]Nathan Kline Institute for Psychiatric Research, Orangeburg, NY, USA

[9]Affiliated Brain Hospital of Guangzhou Medical University, Guangzhou 510370, China

[10]The First Affiliated Hospital of Jinan University, Guangzhou, Guangdong 250024, China

[11]Department of Radiology, The First Affiliated Hospital, College of Medicine, Zhejiang University, Hangzhou, Zhejiang 310058, China

[12]Huaxi MR Research Center (HMRRC), Department of Radiology, West China Hospital of Sichuan University, Chengdu, Sichuan 610044, China

[13]Research Unit of Psychoradiology, Chinese Academy of Medical Sciences, Chengdu, Sichuan 610052, China

[14]Department of Psychiatry, First Affiliated Hospital of Kunming Medical University, Kunming, Yunnan 650032, China

[15]Sino-Danish College, University of Chinese Academy of Sciences, Beijing 101408, China

[16]Sino-Danish Center for Education and Research, Graduate University of Chinese Academy of Sciences, Beijing 101408, China

[17]Department of Psychiatry, and National Clinical Research Center for Mental Disorders, The Second Xiangya Hospital of Central South University, Changsha 410011, Hunan, China

[18]Department of Neurology, Affiliated ZhongDa Hospital of Southeast University, Nanjing, Jiangsu 210009, China

[19]Department of Psychiatry, The First Affiliated Hospital of Chongqing Medical University, Chongqing 400042, China

[20]Department of Clinical Psychology, Suzhou Psychiatric Hospital, The Affiliated Guangji Hospital of Soochow University, Suzhou, Jiangsu 215003, China

[21]Xijing Hospital of Air Force Military Medical University, Xi'an, Shaanxi 710032, China

[22]Beijing Anding Hospital, Capital Medical University, Beijing 100120, China

[23]Affiliated Mental Health Center & Hangzhou Seventh People's Hospital, Zhejiang University School of Medicine, Hangzhou, Zhejiang 310063, China

[24]Mental Health Center and Psychiatric Laboratory, West China Hospital of Sichuan University, Chengdu,

Sichuan 610044, China

[25]Department of Psychosomatics and Psychiatry, Zhongda Hospital, School of Medicine, Southeast University, Nanjing, Jiangsu 210009, China

[26]Shenzhen Kangning Hospital, Shenzhen, Guangzhou 518020, China

[27]Faculty of Psychology, Southwest University, Chongqing 400715, China

[28]National Clinical Research Center for Mental Disorders (Peking University Sixth Hospital) & Key Laboratory of Mental Health, Ministry of Health (Peking University), Beijing 100191, China

[29]Xi'an Central Hospital, Xi'an, Shaanxi 710004, China

[30]Institute of Neuroscience, Chongqing Medical University, Chongqing 400016, China

[31]Chongqing Key Laboratory of Neurobiology, Chongqing 400000, China

[32]Department of Neurology, The First Affiliated Hospital of Chongqing Medical University, Chongqing 400042, China

[33]Department of Radiology, The First Affiliated Hospital of Anhui Medical University, Hefei 230022, China

[34]Research Center of Clinical Medical Imaging, Anhui Province, Hefei 230032, China

[35]Anhui Provincial Institute of Translational Medicine, Hefei 230032, China

[36]West China Hospital of Sichuan University, Chengdu, Sichuan 610044, China

[37]Center for Cognition and Brain Disorders, The Affiliated Hospital of Hangzhou Normal University, Hangzhou, Zhejiang 310018, China

[38]Zhejiang Key Laboratory for Research in Assessment of Cognitive Impairments, Hangzhou, Zhejiang 310000, China

[39]First Hospital of Shanxi Medical University, Taiyuan, Shanxi 030001, China

[40]Developmental Population Neuroscience Research Center, IDG/McGovern Institute for Brain Research, Beijing Normal University, Beijing 100091, China

[41]National Basic Science Data Center, Beijing 100038, China

[42]Department of Psychiatry, Sir Run Run Shaw Hospital, Zhejiang University School of Medicine, Hangzhou 310020, Zhejiang, China

[43]Shanghai Mental Health Center, Shanghai Jiao Tong University School of Medicine, Shanghai 200030, China

[44]Department of Diagnostics, Affiliated Hospital, Hangzhou Normal University Medical School,

Hangzhou, Zhejiang 311121, China

[45]Department of Psychiatry, First Affiliated Hospital, China Medical University, Shenyang, Liaoning 110122, China

[46]Early Intervention Unit, Department of Psychiatry, Affiliated Nanjing Brain Hospital, Nanjing Medical University, Nanjing 210024, China

[47]Department of Neurology, The First Affiliated Hospital of Anhui Medical University, Hefei, Anhui 230022, China

[48]Department of Psychiatry, Shanghai Jiao Tong University School of Medicine, Shanghai 200025, China

*Corresponding author:

Chao-Gan Yan, Ph. D.

CAS Key Laboratory of Behavioral Science, Institute of Psychology, Beijing, China

16 Lincui Road, Chaoyang District, Beijing 100101, China

Tel: +86-10-64101582

E-mail: yancg@psych.ac.cn

[#]DIRECT consortium: Chao-Gan Yan, Ph.D.[1,2,3,4,15,16], Xiao Chen, Ph.D.[1,2,3,4,5], Li-Ping Cao, M.D.[9], Wei Chen, M.D.[42], Yu-Qi Cheng, M.D.[14], Yi-Ru Fang, M.D.[43], Qi-Yong Gong, M.D.[12,13], Wen-Bin Guo, M.D.[17], Li Kuang, M.D.[19], Bao-Juan Li, M.D.[21], Tao Li, M.D.[23,24], Yan-Song Liu, M.D.[20], Zhe-Ning Liu, M.D.[17], Jian-Ping Lu, M.D.[26], Qing-Hua Luo, M.D.[19], Hua-Qing Meng, M.D.[19], Dai-Hui Peng, M.D.[43], Jiang Qiu, Ph.D.[27], Yue-Di Shen, M.D.[44], Tian-Mei Si, M.D.[28], Yan-Qing Tang, M.D.[45], Chuan-Yue Wang, M.D.[22], Fei Wang, M.D.[45,46], Hua-Ning Wang, M.D.[21], Kai Wang, M.D.[47], Xiang Wang, M.D.[17], Ying Wang, M.D.[10], Xiao-Ping Wu, M.D.[29], Chun-Ming Xie, M.D.[18], Guang-Rong Xie, M.D.[17], Peng Xie, M.D.[30,31,32], Xiu-Feng Xu, M.D.[14], Hong Yang, M.D.[11], Jian Yang, M.D.[31], Shu-Qiao Yao, M.D.[17], Yong-Qiang Yu, M.D.[33,34,35], Yong-Gui Yuan, M.D.[25], Ke-Rang Zhang, M.D.[39], Wei Zhang, M.D.[36], Zhi-Jun Zhang, M.D.[18], Jun-Juan Zhu, M.D.[48], Xi-Nian Zuo, Ph.D.[40,41], Jing-Ping Zhao, M.D.[17], Yu-Feng Zang, M.D.[37,38]

Abstract

The subgenual anterior cingulate cortex (sgACC) appears to play a central role in the pathophysiology of major depressive disorder (MDD). To wit, its functional interactive profile with the left dorsal lateral prefrontal cortex (DLPFC) has been shown to be related to treatment outcomes with transcranial magnetic stimulation (TMS) treatment outcomes. Nevertheless, previous research on sgACC functional connectivity (FC) in MDD has yielded inconsistent results, partly due to small sample sizes and limited statistical power of prior work. Here, leveraging a large multi-site sample (1660 MDD patients vs. 1341 healthy controls) from Phase II of the Depression Imaging REsearch ConsorTium (DIRECT), we systematically delineated case-control difference maps of sgACC FC and examined their clinical relevance to previously identified TMS targets. We also investigated case-control FC difference maps of left DLPFC sub-fields. In MDD patients we found significantly increased FC between sgACC and thalamus and reduced FC to a broad array of brain regions, including somatosensory area, occipital lobe, medial and lateral temporal lobe, and insular cortex, when global signal regression (GSR) was not implemented. Intriguingly, we found enhanced left DLPFC-sgACC FC in MDD patients when GSR was performed. We leveraged an prior independent sample to explore the possible relationship between the case-control differences regarding sgACC's FC profiles and the treatment out comes of TMS. In sites in which open TMS treatment was administered, case-control differences in sgACC FC, with GSR, were related to clinical improvement. Next we tested whether the position of peak of the FC maps (previously identified TMS target) could be altered in MDD patients as compred with healthy controls (HC)s. We found the optimized TMS target differed in MDD patients. Several DLPFC sub-fields yielded case-control differences in whole-brain FC maps. In summary, we reliably delineated MDD-related abnormalities of sgACC FC profiles in a large sample. GSR was essential in applying case-control difference maps to identify optimized TMS targets. Our results highlight the functional heterogeneity of the left DLPFC and of precise TMS targets therein.

Keywords: major depressive disorder, transcranial magnetic stimulation, functional connectivity, global signal regression

Introduction

Major depressive disorder (MDD) is a common and debilitating psychiatric disorder projected to be the most burdensome worldwide within this decade (1). Despite extensive research, the pathophysiology of MDD remains elusive. Nevertheless, a key locus appears to be the subgenual anterior cingulate cortex (sgACC), which shows reproducible metabolic hyperactivity (2), is targeted in deep brain stimulation (3, 4), and has been implicated in emotional responses, motivation, and rumination (5). Furthermore, identifying an optimized neuromodulation target in the left dorsal lateral prefrontal cortex (DLPFC) on the basis of sgACC-related functional connectivity (FC) and understanding MDD-related functional abnormalities in DLPFC sub-fields are considered crucial for developing effective depression treatments (6, 7). However, given inconsistent results from small sample-sized studies (8-14), we set out to establish a large sample in which we could seek to identify reliable abnormalities in sgACC and DLPFC FC and better understand the potential impact of such FC profiles on neuromodulation target identification for treating depression.

Multiple studies have investigated FC abnormalities in MDD using resting-state functional magnetic resonance imaging (rsfMRI). Abnormal FC between sgACC and amygdala, thalamus, temporal gyrus, lingual gyrus, cerebellum, dorsal lateral prefrontal cortex (DLPFC), and default mode network (DMN) regions such as medial and dorsal medial prefrontal cortex, precuneus, and parahippocampus have been reported (8, 9, 12-19). However, results have been highly inconsistent, making it challenging to integrate findings and generate clear profiles of sgACC-related FC abnormalities. Such lack of reproducibility could be partially due to small sample size and low statistical power of clinical imaging studies (20, 21). Another possible reason is the implementation of global signal regression (GSR). GSR is the removal of the mean signal averaged across the entire brain via linear regression and one of the most controvirtial preprocessing steps in rsfMRI (22, 23). On the one hand, GSR can increase the specificity of FC by efficiently reducing the impact of non-neuronal nuisance variables, such as head motion and respiration (24, 25). On the other hand, GSR has been criticized for artificially shifting the

168 distribution of the originally derived FCs and introducing spurious anti-correlations (26).
169 Accordingly, not all previous studies implemented GSR, which might significantly alter case-
170 control comparison results (27).
171
172 Maps of sgACC-related FC abnormalities may be clinically useful for predicting repetitive
173 transcranial magnetic stimulation (rTMS) treatment outcomes (28-30). Specifically, the anti-
174 correlation between sgACC and left DLPFC has been associated with clinical improvement after
175 receiving rTMS treatment (31-35). This has led to the intriguing notion that the FC between
176 sgACC and left DLPFC could be leveraged to identify more precise rTMS targets and improve
177 the efficacy of rTMS delivered to the left DLPFCr (6, 36). Indeed, a group-wise sgACC target has
178 been identified (33), and several individualized FC-guided TMS target identification algorithms
179 have been proposed following this rationale (36-39). It is worth noting that the existing sgACC
180 group target was based on the functional connectome of a large cohort of healthy adults.
181 Subtle but significant case-control differences in resting-state FC profiles have been identified
182 in a large sample of MDD patients (40). Thus, understanding the profiles of sgACC FC map case-
183 control differences and their impact on potential targets of rTMS to the left DLPFC could be a
184 critical step toward developing optimized rTMS site identification methods.
185
186 The left DLPFC is an anatomically extensive region consisting primarily of two Brodmann areas
187 (BA 9 and BA 46) (41). Several rTMS targeting approaches have been implemented in the
188 literature, including 1) scalp-based measures ("5 cm" method and F3 Beam method); 2)
189 anatomical targeting (leveraging neuro-navigation to target an anatomical coordinate in BA 9
190 or BA 46); and 3) group-wise connectivity-based targets (the anti-correlation peak of the
191 group-wise mean FC map) (6, 33, 42-44). These methods have generated multiple TMS target
192 sites, with the result that the location of an optimal left DLPFC TMS target remains unsettled.
193 Evaluating case-control differences of common rTMS sites' FC maps might help delineate the
194 MDD-related functional abnormalities of various DLPFC sub-fields.
195
196 To address the issue of sample-size, we initiated the Depression Imaging REsearch ConsorTium

197 (DIRECT) (45) and and carried out an initial meta/mega-analysis (N_{MDD} = 1300), referred to as
198 REST-meta-MDD (40). Studies from the initially shared DIRECT data revealed multiple MDD-
199 related abnormalities including in network FC, whole-brain FC topological and dynamic
200 features, and functional lateralization (40, 46-52). The DIRECT Phase I neuroimaging data were
201 preprocessed using a volume-based approach (DPARSF (53, 54)), producing voxel-wise BOLD
202 time series at each participating hospital which were then shared. In the second phase of
203 DIRECT, we pooled a larger MDD sample (N_{MDD} = 1660) which was preprocessed with a state-
204 of-the-art pipeline, DPABISurf (55). DIRECT Phase II will share voxel/vertex level BOLD time
205 series, allowing more flexible and thorough investigations. The aim of the current study is
206 threefold, to: 1) leverage this highly powered sample to derive a reliable sgACC-related FC
207 abnormality profile in MDD; 2) evaluate the potential impact of such an abnormality on rTMS
208 target identification and explore its potential clinical usage; 3) delineate MDD-related FC
209 abnormalities of commonly used rTMS localization methods within the left DLPFC.
210

211 ## Materials and Methods

212 ### Study sample

213 The DIRECT Phase II initiative comprises 23 cohorts and includes rsfMRI and T1 structural scans
214 from 1660 MDD patients and 1341 HCs. Demographic and clinical characteristics for each
215 sample are presented in Figure 1. Site information, sample size, and previous publications
216 based on the shared data are listed in Table S1. Patients were diagnosed with MDD based on
217 ICD 10 or DSM-IV. All participants provided written informed consent, and local institutional
218 review boards approved each study from all included cohorts.

219 ### Image preprocessing

220 Acquisition parameters and scanners for all cohorts are provided in Table S2. All rsfMRI and
221 structural MRI scans were preprocessed at each site using the same DPABISurf protocol, an
222 rsfMRI data analysis toolbox evolved from DPABI/DPARSF (53-55) (For details, see SI).

Computation of sgACC and DLPFC FC maps

Although recent studies have attempted to identify personalized TMS targets using surface-based algorithms (37), most previous studies have reported targets in volume-based MNI space with sgACC ROIs defined as a sphere in volume-based space (31, 56). To better compare our results with the existing literature, we used the volume-based preprocessed imaging data from DPABISurf.

Because no consensus has been achieved on the anatomical definition of the sgACC, we tested two sets of definitions: (1) a 10 mm sphere located on the average MNI coordinates based on prior studies showing reduced glucose metabolism or blood flow after receiving an antidepressant treatment (MNI coordinates: x = 6, y = 16, z = -10. For details, please refer to Fox et al., 2012 (31).); and (2) a mask denoting the anatomical boundary of BA 25 (57).

Two BA areas in the DLPFC, BA9 and BA46, have been proposed to correspond to different FC profiles. As a result, we defined a priori ROIs by placing 20 mm spheres centered along the left hemisphere at BA9 (MNI coordinates: x = -36, y = 39, z = 43) and BA46 (MNI coordinates: x = -44, y = 40, z = 29) (6). Additionally, we evaluated several TMS targets from the literature: 1) the “5 cm” method (MNI coordinates: x = -41, y = 16, z = 54) (36); 2) the F3 Beam group-average target (MNI coordinates: x = −37, y = 26, z = 49) (29); and 3) the sgACC group target (MNI coordinates: x = −42, y = 44, z = 30) (33).

The time series of sgACC and DLPFC were determined for each individual by spatially averaging the preprocessed rsfMRI time series across all voxels in the above-mentioned masks . We then calculated whole-brain FC maps in volume-based MNI space. FC was calculated using Pearson’s correlation and underwent Fisher’s r-to-z transformation. All FC maps were smoothed with a 6 mm full-width half maximum (FWHM) kernel size.

Harmonization of batch effects

We used ComBat (58) to control potential site and scanner biases. ComBat models site-specific scaling factors by introducing terms for biological variables and scanners in a multivariate linear mixed effects regression. By employing empirical Bayesian criteria, it improves the estimation of studies with small sample sizes. ComBat assumes that the expected FC value can be modeled as a linear combination of batch effects and biological effects. Specifically, the error term in this model is modulated by additional site-specific scaling factors. Let y denote a given FC value:

$$y = \alpha + X^T\beta + \gamma + \delta\varepsilon \tag{1}$$

where $\boldsymbol{\alpha}$ denotes the constant term; X^T denotes the design matrix for covariates of interest (diagnosis, age, sex, education, head motion); $\boldsymbol{\beta}$ is a vector of regression coefficients corresponding to X; $\boldsymbol{\gamma}$ stands for addictive site effects (location parameter) while $\boldsymbol{\delta}$ represents multiplicative site effects (scale parameter). Accordingly, harmonized FC values were defined as:

$$y^{ComBat} = \frac{y-\hat{\alpha}-X^T\hat{\beta}-\hat{\gamma}}{\hat{\delta}} + \alpha + X^T\hat{\beta} \tag{2}$$

where $\hat{\delta}$ and $\hat{\gamma}$ stand for the empirical Bayesian estimates of $\boldsymbol{\delta}$ and $\boldsymbol{\gamma}$, respectively. y^{ComBat} was calculated with the "yw_Harmonization" function in DPABISurf (http://rfmri.org/DPABISurf). ComBat models biological and non-biological effects and algebraically removes the estimated additive and multiplicative batch effects.

Group difference maps

We used a generalized linear model (GLM) to examine differences in the FC maps of sgACC and DLPFC seeds between MDD patients and HCs. Cohen's f^2 was also calculated to characterize effect sizes of this group difference effect. The GLM model includes age, sex, education, and head motion as covariates:

$$\boldsymbol{y} = \boldsymbol{\mu} + \boldsymbol{X\beta} + \boldsymbol{\epsilon} \tag{3}$$

where y denotes the FC value of a given voxel from a given participant; $\boldsymbol{\mu}$ stands for the

275 constant term; X represents the design matrix for the covariates of interest (diagnosis, age, sex,
276 education, and head motion); $\boldsymbol{\beta}$ is a vector of regression coefficients corresponding to X; and
277 $\boldsymbol{\epsilon}$ is a vector of residuals that follow $N(0, \boldsymbol{\sigma}^2)$. Multiple comparison correction was conducted
278 using false discovery rate (FDR) correction at $q < 0.05$.

279 **Group difference targets**

280 We first defined a left DLPFC ROI by combining four 20 mm radius spheres centered in BA9
281 (MNI coordinates: x = -36, y = 39, z = 43), BA46 (MNI coordinates: x = -44, y = 40, z = 29), the
282 "5 cm" method site (MNI coordinates: x = -44, y = 40, z = 29), and the F3 Beam site (MNI
283 coordinates: x = −37, y = 26, z = 49) (37). Then we identified the continuous clusters that
284 survived FDR correction within this DLPFC ROI and used the peaks of these clusters as the
285 "group difference target."

286 **Correlation between group differences and clinical efficiency**

287 An openly shared dataset was leveraged to explore the clinical relevance of our present
288 findings (33). This dataset comprises 25 medication resistant MDD patients who underwent 4
289 to 7 weeks of daily repetitive TMS applied over the left DLPFC. Patients' TMS sites were
290 recorded using their structural MRI images and a frameless neuronavigation system.
291 Treatment response was assessed with the 24-item Hamilton Depression Rating Scale (HAMD).
292 We only used the shared MNI coordinates of TMS sites and the corresponding reductions in
293 HAMD scores from each patient. For more details of this dataset, please refer to Weigand et
294 al. (33). We first extracted the mean t-values of 4 mm radius spheres centered on the TMS
295 sites, then examined the Pearson correlations between these t-values and HAMD score
296 reductions.

297 **sgACC group target in MDD and HC**

298 Since the existing sgACC group target was identified using a cohort of healthy young adults (33)
299 and the significant FC profile differences between MDD and HC (59), we searched for the peak

300 sgACC anti-correlation within the abovementioned DLPFC ROIs in both MDD and HC groups.
301 We first averaged whole-brain FC maps across all MDD patients and HCs, then simply searched
302 for the peak anticorrelated voxel to define the putative target site.

303 **Clustering of DLPFC group difference FC maps**

304 Given the similarities among some DLPFC ROI group difference FC maps, we sought to identify
305 common clusters using Ward's hierarchical clustering method (60). Specifically, spatial
306 correlations were calculated between each pair of group difference *t* maps of DLPFC FC profiles,
307 with the maps that showed the largest similarity grouped into clusters. We evaluated the
308 strength of clustering with the gap statistic (61).

309 **Network-wise group differences**

310 To further interpret group difference maps, we extracted the mean FC values of seven
311 networks using Schaefer's 400 parcellation atlas (62). A GLM model identical to model (3) was
312 constructed to characterize case-control differences for each network. Bonferroni multiple
313 comparison correction was conducted ($p < 0.05/7$). All codes have been made openly available
314 (https://github.com/Chaogan-Yan/PaperScripts/tree/master/Chen_2023). Image results were
315 rendered on the brain surface using BrainNet Viewer (63). Statistics represented in graphical
316 format were generated in R GNU v4.2.1 using the" ggplot" package (64, 65).
317

318 **Results**

319 **Group difference maps of sgACC FC**

320 We found significant MDD-related hyperconnectivity with the sgACC in bilateral DLPFC,
321 temporal parietal junction and occipital lobe, as well as hypoconnectivity in bilateral temporal
322 lobe, left inferior frontal gyrus and left postcentral gyrus when preprocessing included GSR.
323 When GSR was not included in preprocessing, MDD-related sgACC FC alterations showed a

predominance of hypoconnectivity. Abnormally decreased FCs were revealed across the central gyrus, occipital lobe, insular cortex, temporal lobe and a small portion of the frontal lobe. Without GSR, MDD-related hyperconnectivity was limited to subcortical regions (Figure 2A). Of note, these results were obtained when the sgACC was defined as a sphere. When a more subtle, anatomically-based definition (a BA 25 mask) was used, no significant MDD-related FC abnormality was detected when GSR was performed. When GSR was not included in preprocessing, hypoconnectivity predominated across the brain, except for subcortical regions, similar to results for the spherical mask (Figure S1). Network-wise FC analyses showed that MDD patients' FC between sgACC and the limbic network (LN) was significantly reduced compared to HC ($t = -4.357$, $p_{corrected} < 0.001$, Cohen's $f^2 = 0.007$). Without GSR, MDD patients showed decreased FC between sgACC and all brain networks (all $p_{corrected} < 0.05$) except for the frontoparietal network (FPN) (Figure 2B).

Correlation between group differences and clinical efficiency

Using an openly shared clinical dataset, we examined the relationship between group differences (t-values) and clinical effects (HAMD score reductions) to test the clinical relevance of group difference maps. Group differences were positively correlated with HAMD score reductions ($r = 0.448$, $p = 0.025$, Figure 2C).

sgACC anti-correlation peaks in MDD and HCs

The above results highlighted the group differences in sgACC FC profiles between MDD and HCs. Since the existing sgACC group target was based on a cohort of young, healthy adults, we sought to examine potential differences of anti-correlation peaks extracted from the mean sgACC FC maps of MDD and HC groups (Figure 3). We found that the anti-correlation peak of MDD patients (MNI coordinates: $x = -46$, $y = 4$, $z = 40$) was more posterior compared to HCs (MNI coordinates: $x = -44$, $y = 38$, $z = 30$), probably due to less anticorrelated FC within the left DLPFC in MDD patients. The anti-correlation peak extracted from HCs was closer to that reported in the existing literature (MNI coordinates: $x = -42$, $y = 44$, $z = 30$).

350 **Identifying the group difference target**

351 We identified two contiguous clusters of voxels that showed significant group differences in
352 the left DLPFC. The peaks of these clusters were defined as target coordinates. Group
353 difference target 1 (MNI coordinates: x = -44, y = 38, z = 32; t = 3.277, p < 0.001, Cohen's f2 =
354 0.004) was ventral to group difference target 2 (MNI coordinates: x = -34, y = 36, z = 40; t =
355 3.670, p < 0.001, Cohen's f2 = 0.005) (Figure 4).

356 **Group difference maps of different DLPFC ROI FC profiles**

357 When GSR was implemented, FC maps for most DLPFC ROIs showed significant MDD-related
358 abnormalities (FDR q < 0.05) except for Group Difference Target 2 and BA 9 (Figure 4A).
359 Although each ROIs' MDD-related abnormality map was unique, these MDD-related
360 abnormality maps demonstrated one of three general topographic patterns (Figure 4B). The
361 gap statistic quantified an optimal three-cluster solution (Figure S2). Cluster 1 included Group
362 Difference Target 1, BA 46, and the sgACC group target. MDD patients showed enhanced FCs
363 between the medial prefrontal cortex, posterior cingulate cortex, temporal parietal junction,
364 and lateral temporal cortex and decreased FCs between the right inferior prefrontal cortex and
365 the DLPFC ROIs. Cluster 2 consisted of Group Difference Target 2 and BA 9. No significant MDD-
366 related abnormalities were revealed. Nevertheless, enhanced FC between the medial
367 orbitofrontal cortex and occipital cortex were observed when a more liberal threshold was
368 implemented (Gaussian random field correction: voxel-wise p < 0.01, cluster-wise p < 0.05,
369 two-tailed). Cluster 3 included the F3 Beam and the "5 cm" Method ROIs. For these, we found
370 enhanced FCs between the dorsal anterior cingulate cortex, insular, and occipital cortex, and
371 reduced FCs between the lateral temporal cortex and posterior cingulate cortex and the DLPFC
372 ROIs in MDD patients compared with HCs.

373 **Group differences of network-wise FC of different DLPFC ROIs**

374 All three clusters showed group differences in distinct network-wise FC patterns (Figure 6).
375 MDD patients showed enhanced FCs between the Default Mode Network (DMN) and three

Cluster 1 ROIs (Group Difference Target 1: $t = 3.483$, $p_{corrected} = 0.004$, Cohen's $f^2 = 0.004$; BA46: $t = 3.791$, $p_{corrected} = 0.001$, Cohen's $f^2 = 0.005$; sgACC group target: $t = 3.810$, $p_{corrected} = 0.001$, Cohen's $f^2 = 0.005$). We only found significantly reduced FC between the Ventral Attention Network (VAN) and the sgACC group target ($t = -3.057$, $p_{corrected} = 0.016$, Cohen's $f^2 = 0.003$) but no significant alterations in two other DLPFC ROIs (all $p_{corrected} > 0.05$). DLPFC Cluster 2 ROIs showed significantly increased LN FC (Group Difference Target 2: $t = 2.753$, $p_{corrected} = 0.042$, Cohen's $f^2 = 0.003$; $t = 2.897$, $p_{corrected} = 0.027$, Cohen's $f^2 = 0.003$). Only Group Difference Target 2 yielded significantly enhanced somatomotor network (SMN) FC ($t = 2.716$, $p_{corrected} = 0.047$, Cohen's $f^2 = 0.003$). The network-wise FC profiles of Cluster 3's DLPFC ROIs were generally similar, but significant FC differences were found in different brain networks. The F3 Beam ROI showed significantly increased FC to the visual network (VN) ($t = 3.032$, $p_{corrected} = 0.017$, Cohen's $f^2 = 0.003$) while the "5 cm" Method ROI showed significantly enhanced FCs to the VAN ($t = 3.512$, $p_{corrected} = 0.003$, Cohen's $f^2 = 0.004$) and reduced FC to the DMN ($t = -2.779$, $p_{corrected} = 0.038$, Cohen's $f^2 = 0.003$).

Discussion

In the present study, we leveraged a large multi-site sample (1660 MDD patients and 1341 HCs) and found abnormal sgACC FC in MDD. Specifically, we found reduced FC between sgACC and a broad array of brain regions when GSR was not conducted, while FC between sgACC and the left DLPFC was enhanced in MDD patients when GSR was implemented. We identified two clusters in the left DLPFC which could serve as potential rTMS treatment targets in depression. In a dataset reporting effects of open rTMS treatment, group differences in sgACC-DLPFC FC were related to clinical improvement. Interestingly, the locations of anti-correlation peaks differed substantially in MDD patients compared to HCs. In examining the group difference maps of various DLPFC ROI FC profiles we found that the DLPFC ROIs could be grouped into three clusters, which also corresponded to network-wise FCs. These results suggest that group differences in sgACC FC may be clinically relevant. As the field moves towards identifying individualized TMS sites, such group differences might be useful for developing next-generation target-localization algorithms.

404 **MDD-related sgACC FC abnormalities**

405 Our results add to a growing literature showing functional network abnormalities involving the
406 sgACC in MDD (8, 10-12, 16, 18, 66-68). Nevertheless, notable discrepancies in the type of
407 abnormality (enhanced/reduced) and specific brain regions showing altered sgACC FCs have
408 been reported. With an unprecedented sample size, our results have provided the most robust
409 evidence to date. However, the effect sizes of MDD-related sgACC FC abnormalities were small
410 (Cohen's $f^2 < 0.01$). The combination of the limited power of small sample sizes in previous
411 studies and a small effect-sized case-control difference were likely to produce false positive
412 findings (20, 69, 70), which may not be able to be reproduced in the present study.
413 Furthermore, we robustly demonstrated that GSR dramatically changed the group difference
414 maps of sgACC FC profiles. GSR is effective at removing non-neuronal physiological noises such
415 as signal contributions from respiratory (71), but can alter the BOLD signal covariances due to
416 its less specific nature (72). One recent study examined the relationship between the sgACC-
417 DLPFC anti-correlation and the treatment outcomes of TMS using a large dataset (THREE-D)
418 (73) and found that such correlation was largely carried by respiration-related signal patterns
419 (32). Accordingly, most prior studies that intended to identify the TMS targets guided by
420 sgACC-related FCs tend to implement GSR to remove the non-neural noises as much as
421 possible, while other studies that were intended to delineate the general case-control
422 differences prefer not to implement GSR. Here, with an unprecendented large sample, we
423 showed that GSR might induce notable alterations in case-control differences of FC maps (27).
424

425 MDD patients showed enhanced FC between sgACC and thalamus regardless of whether GSR
426 was implemented. This result is consistent with previous studies in adolescents (18) and adults
427 (56) with MDD. We found decreased FC between sgACC and the limbic network both with and
428 without GSR. Previous studies have reported abnormal FCs between sgACC and limbic areas
429 and some subcortical regions, such as the amygdala (8, 19) and parahippocampus regions (12).
430 Together, these results are consistent with a model highlighting sgACC as a critical hub in an
431 "extended medial network," which also encompasses limbic, thalamic, and striatal regions and

432 plays a key role in the pathophysiology of MDD (74, 75). This “extended medial network”
433 overlaps substantially with the DMN. Indeed, decreased FCs between sgACC and DMN regions,
434 such as the medial prefrontal cortex, precuneus, temporal gyrus, and parahippocampus
435 regions, were revealed in MDD relative to HCs when GSR was not implemented. Such
436 abnormalities have been previously reported (9, 11, 14, 29), which led to the hypothesis that
437 abnormally enhanced FC between sgACC and DMN are the network underpinnings of
438 rumination (76). However, inconsistent with the prediction of this model, we found reduced,
439 instead of enhanced FC between sgACC and DMN. Based on a large multi-site sample of MDD
440 patients from the first phase of DIRECT, we previously demonstrated that MDD was
441 characterized by reduced FC within DMN (40, 45). One notable issue is that both the first phase
442 and the current second phase of the DIRECT data were solely comprised of Chinese samples,
443 while most studies reporting enhanced sgACC-DMN FCs in MDD recruited Caucasian samples.
444 Different prevalence rates (77, 78), heterogeneous symptoms (79), and different risk alleles
445 (80) have been reported in Caucasian and Eastern Asian groups. As a result, racial differences
446 may have contributed to this discrepancy.

447 **Clinical relevance of MDD-related sgACC FC abnormalities**

448 Although case-control comparisons must be interpreted with caution when GSR has been
449 implemented, our results support the clinical relevance of such analyses with regard to rTMS
450 treatment outcomes. Substantial evidence has shown that sgACC FC profiles in MDD patients
451 are related to rTMS treatment response (30, 81). Our results add to this conceptualization by
452 showing that the degree of group differences in the sgACC FC profiles were positively related
453 to the clinical improvements after receiving rTMS to the left DLPFC. Normative connectome
454 datasets have been used to identify group-wise anti-correlation peaks as TMS targets (31, 33,
455 36). Here, we found that the locations of such anticorrelated peaks can differ substantially in
456 a large clinical cohort. Specifically, FC of the more anterior part of the left DLPFC was
457 abnormally elevated in MDD patients, and thus less anticorrelated to sgACC relative to HCs,
458 which resulted in a more posterior peak in patients than in HCs.
459

460 Interestingly, the thresholded group difference maps revealed two clusters showing enhanced
461 FC to sgACC in the left DLPFC. Philip and colleagues reported that the FC between the left
462 DLPFC and sgACC were reduced after receiving 40 daily sessions of 5 Hz TMS to the left DLPFC.
463 Such a reduction in FC was also related to reduced self-reported symptom scores (30).
464 Identifying optimum targets in the left DLPFC from multiple clusters is challenging (37).
465 Spherical ROIs centered at the peaks of these two clusters corresponded to different FC
466 profiles and group difference maps. Criteria to determine the optimal target might require
467 more benchmarking using clinical data. Defining a reliable TMS target solely based on one
468 individual's rsfMRI data (typical duration ~8 mins in clinical practice) is challenging. The
469 replicability of FC derived from fMRI images is poor (82), and current available individual-level
470 network parcellation algorithms often require a large number of fMRI images (usually more
471 than one hour) (83). Given the high reliability of group difference maps derived from a large
472 sample ($N_{patients}$ > 1500), it might be possible to leverage this map to generate better group
473 based targets and improve outcomes in the clinical practice.

474 **Different functional network profiles of different DLPFC ROIs**

475 Most clinical trials have focused on applying TMS to the left DLPFC with the belief that high-
476 frequency rTMS can enhance hypoactivity during depressive episodes (7, 84). The DLPFC is
477 anatomically extensive but it can be represented by BA 46 and BA 9 (41). It remains unclear
478 which DLPFC sub-field is the best target for TMS. The current FDA-approved protocol (i.e., "5
479 cm" method) results in different stimulation sites in DLPFC for different patients, which may
480 contribute to the heterogeneity in the effect sizes of antidepressant responses in prior trials
481 (85, 86). In the current study, we underscore the potential importance of individualized,
482 precise identification of stimulation sites for rTMS by showing that different DLPFC ROIs
483 correspond to different group difference FC profiles. In line with our findings, Siddiqi and
484 colleagues found that the correlation maps between stimulations' connectomes and symptom
485 responses could be grouped into two clusters, indicating that different response patterns are
486 related to different TMS targets (87). Our results regarding network-wise FC suggest that BA
487 46 is hyperconnected to the DMN while BA 9 is hyperconnected to the LN in MDD relative to

488 HCs. The DMN has been proposed to be involved in pathological ruminations (76) that can
489 occur in some patient with MDD, while the LN might be related to anhedonia, decreased
490 motivation, and changes in sleep and appetite patterns (3). We speculate that stimulating one
491 site might be effective for a specific sub-group of patients with a particular cluster of symptoms
492 (e.g., rumination vs. anhedonia) while other patients might not respond. We note that
493 leveraging anatomical landmarks to precisely target the boundary between BA 9 and BA 46 did
494 not consistently outperform the "5 cm" method or the F3 Beam method (88, 89). Our results
495 suggest that the FC profiles of these two regions could be a critical factor in determining the
496 treatment outcome of TMS.

497 **Definition of sgACC**

498 It may seem counterintuitive that only spherical-defined sgACC could generate significant
499 group difference maps when GSR was implemented. We note that the anatomical definition
500 of the sgACC remains controversial. The sgACC was first implicated in the physiopathology of
501 MDD based on its increases glucose metabolism (90) and rsfMRI FCs (9) in MDD patients who
502 a re not respondent to anti-depressant medications and a general reduction in glucose
503 metabolism (91) and blood flow (92) after anti-depressant treatments (93). Most evidence
504 supporting this hypothesis come from functional imaging research (e.g., PET, fMRI). As a result,
505 the brain region showing abnormal metabolism or blood flow may not overlap precisely with
506 the anatomical landmarks of BA 25. Thus, a less specific definition of sgACC (i.e., a sphere) may
507 better capture the brain region in which functional activity is altered, despite its lower
508 anatomic accuracy. Recent studies have applied a more sophisticated targeting algorithm that
509 searched for smaller sub-units within the broader anatomical sgACC region and led to
510 markedly improved treatment outcome (39). Another issue is the poor signal-to-noise ratio of
511 sgACC in fMRI (94). Calculating whole-brain FC maps between one given subject's sgACC and
512 a large independent cohort (so-called "seed map") and then using this seed map to substitute
513 the sgACC seed region may help address this issue and generate a more reproducible DLPFC
514 target (36, 37). Further research is needed to develop the optimal way to define the sgACC in
515 clinical practice.

516 **Limitations**

517 Several limitations need to be considered. First, we noted that the inconsistency between our
518 results and the broader literature could partly be due to racial differences of the samples (i.e.,
519 Eastern Asian vs. Caucasian). Consortiums that intend to pool existing neuroimaging data
520 worldwide, such as the Enhancing NeuroImaging Genetics through Meta-Analysis (ENIGMA)
521 Major Depressive Disorder (MDD) consortium (46), have accumulated large-scale data
522 primarily from Western countries and published several high-impact studies delineating MDD-
523 related anatomical abnormalities (95, 96). Future collaborations between the DIRECT and the
524 ENIGMA-MDD consortiums may help address potential cultural, genetic, and environmental
525 mechanisms involved in more diverse groups of MDD patients. Second, the current study
526 applied a volume-based preprocessing approach to facilitate comparison with previous
527 literature. Surface-based preprocessing strategies have provided more accurate and detailed
528 representations of cortical and subcortical structures (97). Recent research has begun to
529 explore surface-based rTMS target identification algorithms and has shown promising clinical
530 relevance (34, 35, 98). Future research should consider using surface-based case-control
531 difference maps to develop new ways to identify TMS targets.

532 **Conclusion**

533 In summary, we leveraged a large sample of MDD patients to fully delineate group differences
534 of sgACC FC maps between MDD patients and HCs. We also evaluated the clinical relevance of
535 TMS treatment outcomes as a function of TMS target sites. Moreover, we considered several
536 common left DLPFC ROIs' case-control comparison results of FC maps, which underscored the
537 functional heterogeneity within the anatomical landmarks of the left DLPFC and highlighted
538 the necessity of identifying individualized DLPFC TMS sites.

539 **Conflict of interest**

540 The authors declare no conflict of interest.

Acknowledgements

This work was funded by the Sci-Tech Innovation 2030 - Major Project of Brain Science and Brain-inspired Intelligence Technology (No. 2021ZD0200600), the National Key R&D Program of China (No. 2017YFC1309902), the National Natural Science Foundation of China (No. 82122035, No. 81671774 and No. 81630031), the 13th Five-year Informatization Plan of Chinese Academy of Sciences (No. XXH13505), the Key Research Program of the Chinese Academy of Sciences (No. ZDBS-SSW-JSC006), Beijing Nova Program of Science and Technology (No. Z191100001119104), the Scientific Foundation of Institute of Psychology, Chinese Academy of Sciences (No. E2CX4425YZ), the China Postdoctoral Science Foundation (No. 2019M660847), the China National Postdoctoral Program for Innovative Talents (No. BX20200360), the Scientific Foundation of Institute of Psychology, Chinese Academy of Sciences (No. Y9CX422005), and the Special Research Assistant Program of the Chinese Academy of Sciences (No. E2CX0624). The support provided by China Scholarship Council (CSC, No. 202104910248) during a visit of Xiao Chen to the Centre for Addiction and Mental Health is acknowledged.

References

1. G. S. Malhi, J. J. Mann, Depression. *Lancet (London, England)* **392**, 2299-2312 (2018).
2. W. C. Drevets, J. L. Price, M. L. Furey, Brain structural and functional abnormalities in mood disorders: implications for neurocircuitry models of depression. *Brain structure & function* **213**, 93-118 (2008).
3. H. S. Mayberg, Modulating dysfunctional limbic-cortical circuits in depression: towards development of brain-based algorithms for diagnosis and optimised treatment. *British medical bulletin* **65**, 193-207 (2003).
4. H. S. Mayberg *et al.*, Deep brain stimulation for treatment-resistant depression. *Neuron* **45**, 651-660 (2005).
5. S. G. Disner, C. G. Beevers, E. A. P. Haigh, A. T. Beck, Neural mechanisms of the cognitive model of depression. *Nat Rev Neurosci* **12**, 467-477 (2011).
6. R. F. H. Cash *et al.*, Using Brain Imaging to Improve Spatial Targeting of Transcranial Magnetic Stimulation for Depression. *Biol Psychiatry* 10.1016/j.biopsych.2020.05.033 (2020).
7. P. B. Fitzgerald, Targeting repetitive transcranial magnetic stimulation in depression: do we really know what we are stimulating and how best to do it? *Brain Stimul* **14**,

730-736 (2021).

8. C. G. Connolly *et al.*, Resting-State Functional Connectivity of Subgenual Anterior Cingulate Cortex in Depressed Adolescents. *Biological Psychiatry* **74**, 898-907 (2013).

9. M. D. Greicius *et al.*, Resting-state functional connectivity in major depression: abnormally increased contributions from subgenual cingulate cortex and thalamus. *Biol Psychiatry* **62**, 429-437 (2007).

10. H. Wu *et al.*, Changed Hub and Corresponding Functional Connectivity of Subgenual Anterior Cingulate Cortex in Major Depressive Disorder. *Front Neuroanat* **10**, 120 (2016).

11. C. G. Davey, B. J. Harrison, M. Yucel, N. B. Allen, Regionally specific alterations in functional connectivity of the anterior cingulate cortex in major depressive disorder. *Psychol Med* **42**, 2071-2081 (2012).

12. B. Cheng *et al.*, Functional connectivity patterns of the subgenual anterior cingulate cortex in first-episode refractory major depressive disorder. *Brain imaging and behavior* **15**, 2397-2405 (2021).

13. Y. I. Sheline, J. L. Price, Z. Yan, M. A. Mintun, Resting-state functional MRI in depression unmasks increased connectivity between networks via the dorsal nexus. *Proc Natl Acad Sci U S A* **107**, 11020-11025 (2010).

14. M. G. Berman *et al.*, Depression, rumination and the default network. *Social cognitive and affective neuroscience* **6**, 548-555 (2011).

15. X. Wu *et al.*, Dysfunction of the cingulo-opercular network in first-episode medication-naive patients with major depressive disorder. *J Affect Disord* **200**, 275-283 (2016).

16. K. Sudheimer *et al.*, Decreased hypothalamic functional connectivity with subgenual cortex in psychotic major depression. *Neuropsychopharmacology* **40**, 849-860 (2015).

17. C. G. Davey, M. Yücel, N. B. Allen, B. J. Harrison, Task-related deactivation and functional connectivity of the subgenual cingulate cortex in major depressive disorder. *Frontiers in psychiatry* **3**, 14 (2012).

18. M. S. Gaffrey *et al.*, Subgenual cingulate connectivity in children with a history of preschool-depression. *Neuroreport* **21**, 1182-1188 (2010).

19. T. C. Ho *et al.*, Functional connectivity of negative emotional processing in adolescent depression. *J Affect Disord* **155**, 65-74 (2014).

20. K. S. Button *et al.*, Power failure: why small sample size undermines the reliability of neuroscience. *Nat Rev Neurosci* **14**, 365-376 (2013).

21. J. Algermissen, D. M. A. Mehler, May the power be with you: are there highly powered studies in neuroscience, and how can we get more of them? *J Neurophysiol* **119**, 2114-2117 (2018).

22. K. Murphy, M. D. Fox, Towards a Consensus Regarding Global Signal Regression for Resting State Functional Connectivity MRI. *Neuroimage* 10.1016/j.neuroimage.2016.11.052 (2016).

23. L. Q. Uddin, Mixed Signals: On Separating Brain Signal from Noise. *Trends Cogn Sci* **21**, 405-406 (2017).

24. M. D. Fox, D. Zhang, A. Z. Snyder, M. E. Raichle, The global signal and observed anticorrelated resting state brain networks. *J Neurophysiol* **101**, 3270-3283 (2009).

616 25. R. Ciric *et al.*, Mitigating head motion artifact in functional connectivity MRI. *Nature*
617 *protocols* **13**, 2801-2826 (2018).
618 26. K. Murphy, R. M. Birn, D. A. Handwerker, T. B. Jones, P. A. Bandettini, The impact of
619 global signal regression on resting state correlations: Are anti-correlated networks
620 introduced? *NeuroImage* **44**, 893-905 (2009).
621 27. L. Parkes, B. Fulcher, M. Yücel, A. Fornito, An evaluation of the efficacy, reliability, and
622 sensitivity of motion correction strategies for resting-state functional MRI.
623 *NeuroImage* **171**, 415-436 (2018).
624 28. R. Ge, J. Downar, D. M. Blumberger, Z. J. Daskalakis, F. Vila-Rodriguez, Functional
625 connectivity of the anterior cingulate cortex predicts treatment outcome for rTMS in
626 treatment-resistant depression at 3-month follow-up. *Brain Stimul* **13**, 206-214 (2020).
627 29. R. F. H. Cash *et al.*, A multivariate neuroimaging biomarker of individual outcome to
628 transcranial magnetic stimulation in depression. *Hum Brain Mapp* **40**, 4618-4629
629 (2019).
630 30. N. S. Philip *et al.*, Network Mechanisms of Clinical Response to Transcranial Magnetic
631 Stimulation in Posttraumatic Stress Disorder and Major Depressive Disorder. *Biol*
632 *Psychiatry* **83**, 263-272 (2018).
633 31. M. D. Fox, R. L. Buckner, M. P. White, M. D. Greicius, A. Pascual-Leone, Efficacy of
634 transcranial magnetic stimulation targets for depression is related to intrinsic
635 functional connectivity with the subgenual cingulate. *Biol Psychiatry* **72**, 595-603
636 (2012).
637 32. I. G. Elbau *et al.*, Functional Connectivity Mapping for rTMS Target Selection in
638 Depression. *Am J Psychiatry* **180**, 230-240 (2023).
639 33. A. Weigand *et al.*, Prospective Validation That Subgenual Connectivity Predicts
640 Antidepressant Efficacy of Transcranial Magnetic Stimulation Sites. *Biol Psychiatry* **84**,
641 28-37 (2018).
642 34. R. F. H. Cash, L. Cocchi, J. Lv, P. B. Fitzgerald, A. Zalesky, Functional Magnetic Resonance
643 Imaging-Guided Personalization of Transcranial Magnetic Stimulation Treatment for
644 Depression. *JAMA psychiatry* **78**, 337-339 (2021).
645 35. S. H. Siddiqi, A. Weigand, A. Pascual-Leone, M. D. Fox, Identification of Personalized
646 Transcranial Magnetic Stimulation Targets Based on Subgenual Cingulate Connectivity:
647 An Independent Replication. *Biol Psychiatry* **90**, e55-e56 (2021).
648 36. M. D. Fox, H. Liu, A. Pascual-Leone, Identification of reproducible individualized targets
649 for treatment of depression with TMS based on intrinsic connectivity. *Neuroimage* **66**,
650 151-160 (2013).
651 37. R. F. H. Cash *et al.*, Personalized connectivity-guided DLPFC-TMS for depression:
652 Advancing computational feasibility, precision and reproducibility. *Hum Brain Mapp*
653 10.1002/hbm.25330 (2021).
654 38. E. J. Cole *et al.*, Stanford Neuromodulation Therapy (SNT): A Double-Blind Randomized
655 Controlled Trial. *Am J Psychiatry* 10.1176/appi.ajp.2021.20101429,
656 appiajp202120101429 (2021).
657 39. E. J. Cole *et al.*, Stanford Accelerated Intelligent Neuromodulation Therapy for
658 Treatment-Resistant Depression. *Am J Psychiatry* **177**, 716-726 (2020).

40. C. G. Yan *et al.*, Reduced default mode network functional connectivity in patients with recurrent major depressive disorder. *Proc Natl Acad Sci U S A* 10.1073/pnas.1900390116 (2019).
41. G. Rajkowska, P. S. Goldman-Rakic, Cytoarchitectonic definition of prefrontal areas in the normal human cortex: II. Variability in locations of areas 9 and 46 and relationship to the Talairach Coordinate System. *Cerebral cortex (New York, N.Y. : 1991)* **5**, 323-337 (1995).
42. W. Beam, J. J. Borckardt, S. T. Reeves, M. S. George, An efficient and accurate new method for locating the F3 position for prefrontal TMS applications. *Brain Stimul* **2**, 50-54 (2009).
43. M. S. George *et al.*, Daily repetitive transcranial magnetic stimulation (rTMS) improves mood in depression. *Neuroreport* **6**, 1853-1856 (1995).
44. M. L. Paillère Martinot *et al.*, Influence of prefrontal target region on the efficacy of repetitive transcranial magnetic stimulation in patients with medication-resistant depression: a [(18)F]-fluorodeoxyglucose PET and MRI study. *The international journal of neuropsychopharmacology* **13**, 45-59 (2010).
45. X. Chen *et al.*, The DIRECT consortium and the REST-meta-MDD project: towards neuroimaging biomarkers of major depressive disorder. *Psychoradiology* **2**, 32-42 (2022).
46. L. Schmaal *et al.*, ENIGMA MDD: seven years of global neuroimaging studies of major depression through worldwide data sharing. *Transl Psychiatry* **10**, 172 (2020).
47. H. Yang *et al.*, Disrupted intrinsic functional brain topology in patients with major depressive disorder. *Mol Psychiatry* 10.1038/s41380-021-01247-2 (2021).
48. Y. Long *et al.*, Altered resting-state dynamic functional brain networks in major depressive disorder: Findings from the REST-meta-MDD consortium. *Neuroimage Clin* **26**, 102163 (2020).
49. Y. D. Ding *et al.*, Disrupted hemispheric connectivity specialization in patients with major depressive disorder: Evidence from the REST-meta-MDD Project. *J Affect Disord* **284**, 217-228 (2021).
50. K. Deng *et al.*, Impaired robust interhemispheric function integration of depressive brain from REST-meta-MDD database in China. *Bipolar disorders* 10.1111/bdi.13139 (2021).
51. S. Liang *et al.*, Biotypes of major depressive disorder: Neuroimaging evidence from resting-state default mode network patterns. *Neuroimage Clin* **28**, 102514 (2020).
52. P. H. Liu *et al.*, Brain structural alterations in MDD patients with gastrointestinal symptoms: Evidence from the REST-meta-MDD project. *Progress in neuro-psychopharmacology & biological psychiatry* **111**, 110386 (2021).
53. C.-G. Yan, X.-D. Wang, X.-N. Zuo, Y.-F. Zang, DPABI: Data Processing & Analysis for (Resting-State) Brain Imaging. *Neuroinformatics* **14**, 339-351 (2016).
54. C.-G. Yan, Y.-F. Zang, DPARSF: A MATLAB Toolbox for "Pipeline" Data Analysis of Resting-State fMRI. *Frontiers in systems neuroscience* **4**, 13 (2010).
55. C.-G. Yan, X.-D. Wang, B. Lu, DPABISurf: data processing & analysis for brain imaging on surface. *Science Bulletin* https://doi.org/10.1016/j.scib.2021.09.016 (2021).

56. C. Liston *et al.*, Default mode network mechanisms of transcranial magnetic stimulation in depression. *Biol Psychiatry* **76**, 517-526 (2014).
57. J. K. Mai, M. Majtanik, *Human Brain in Standard MNI Space: A Comprehensive Pocket Atlas* (Elsevier Science, 2017).
58. W. E. Johnson, C. Li, A. Rabinovic, Adjusting batch effects in microarray expression data using empirical Bayes methods. *Biostatistics* **8**, 118-127 (2007).
59. C. G. Yan *et al.*, Reduced default mode network functional connectivity in patients with recurrent major depressive disorder. *Proc Natl Acad Sci U S A* **116**, 9078-9083 (2019).
60. F. Murtagh, P. Legendre, Ward's Hierarchical Agglomerative Clustering Method: Which Algorithms Implement Ward's Criterion? *Journal of Classification* **31**, 274-295 (2014).
61. R. Tibshirani, G. Walther, T. Hastie, Estimating the number of clusters in a data set via the gap statistic. *Journal of the Royal Statistical Society: Series B (Statistical Methodology)* **63**, 411-423 (2001).
62. A. Schaefer *et al.*, Local-Global Parcellation of the Human Cerebral Cortex from Intrinsic Functional Connectivity MRI. *Cerebral cortex (New York, N.Y. : 1991)* **28**, 3095-3114 (2018).
63. M. Xia, J. Wang, Y. He, BrainNet Viewer: a network visualization tool for human brain connectomics. *PLoS One* **8**, e68910 (2013).
64. R. Computing, R: A language and environment for statistical computing. *Vienna: R Core Team* (2013).
65. R. A. M. Villanueva, Z. J. Chen (2019) ggplot2: elegant graphics for data analysis. (Taylor & Francis).
66. M. Greicius, Resting-state functional connectivity in neuropsychiatric disorders. *Current opinion in neurology* **21**, 424-430 (2008).
67. K. R. Cullen *et al.*, A preliminary study of functional connectivity in comorbid adolescent depression. *Neuroscience Letters* **460**, 227-231 (2009).
68. C. Strikwerda-Brown *et al.*, Mapping the relationship between subgenual cingulate cortex functional connectivity and depressive symptoms across adolescence. *Social cognitive and affective neuroscience* **10**, 961-968 (2015).
69. J. P. A. Ioannidis, Why Most Published Research Findings Are False. *PLOS Medicine* **2**, e124 (2005).
70. X. Chen, B. Lu, C. G. Yan, Reproducibility of R-fMRI metrics on the impact of different strategies for multiple comparison correction and sample sizes. *Hum Brain Mapp* **39**, 300-318 (2018).
71. J. D. Power, M. Plitt, T. O. Laumann, A. Martin, Sources and implications of whole-brain fMRI signals in humans. *Neuroimage* **146**, 609-625 (2017).
72. M. F. Glasser *et al.*, Using temporal ICA to selectively remove global noise while preserving global signal in functional MRI data. *Neuroimage* **181**, 692-717 (2018).
73. D. M. Blumberger *et al.*, Effectiveness of theta burst versus high-frequency repetitive transcranial magnetic stimulation in patients with depression (THREE-D): a randomised non-inferiority trial. *Lancet (London, England)* **391**, 1683-1692 (2018).
74. J. L. Price, W. C. Drevets, Neurocircuitry of mood disorders. *Neuropsychopharmacology* **35**, 192-216 (2010).

745 75. J. L. Price, W. C. Drevets, Neural circuits underlying the pathophysiology of mood
746 disorders. *Trends Cogn Sci* **16**, 61-71 (2012).
747 76. J. P. Hamilton, M. Farmer, P. Fogelman, I. H. Gotlib, Depressive Rumination, the Default-
748 Mode Network, and the Dark Matter of Clinical Neuroscience. *Biol Psychiatry* **78**, 224-
749 230 (2015).
750 77. G. Parker, B. Chan, D. Hadzi-Pavlovic, Lower rates of depression in westernised Chinese
751 in the US. *J Affect Disord* **104**, 175-178 (2007).
752 78. G. Parker, G. Gladstone, K. T. Chee, Depression in the planet's largest ethnic group: the
753 Chinese. *Am J Psychiatry* **158**, 857-864 (2001).
754 79. P. Qiu, E. D. Caine, F. Hou, C. Cerulli, M. N. Wittink, Depression as seen through the
755 eyes of rural Chinese women: Implications for help-seeking and the future of mental
756 health care in China. *J Affect Disord* **227**, 38-47 (2018).
757 80. C. Kiyohara, K. Yoshimasu, Association between major depressive disorder and a
758 functional polymorphism of the 5-hydroxytryptamine (serotonin) transporter gene: a
759 meta-analysis. *Psychiatr Genet* **20**, 49-58 (2010).
760 81. R. Ge *et al.*, Predictive Value of Acute Neuroplastic Response to rTMS in Treatment
761 Outcome in Depression: A Concurrent TMS-fMRI Trial. *Am J Psychiatry*
762 10.1176/appi.ajp.21050541, appiajp21050541 (2022).
763 82. X.-N. Zuo, X.-X. Xing, Test-retest reliabilities of resting-state FMRI measurements in
764 human brain functional connectomics: A systems neuroscience perspective.
765 *Neuroscience & Biobehavioral Reviews* **45**, 100-118 (2014).
766 83. D. Wang *et al.*, Parcellating cortical functional networks in individuals. *Nat Neurosci* **18**,
767 1853-1860 (2015).
768 84. P. B. Fitzgerald *et al.*, An analysis of functional neuroimaging studies of dorsolateral
769 prefrontal cortical activity in depression. *Psychiatry Res* **148**, 33-45 (2006).
770 85. K. A. Johnson *et al.*, Prefrontal rTMS for treating depression: location and intensity
771 results from the OPT-TMS multi-site clinical trial. *Brain Stimul* **6**, 108-117 (2013).
772 86. T. Perera *et al.*, The Clinical TMS Society Consensus Review and Treatment
773 Recommendations for TMS Therapy for Major Depressive Disorder. *Brain Stimul* **9**,
774 336-346 (2016).
775 87. S. H. Siddiqi *et al.*, Distinct Symptom-Specific Treatment Targets for Circuit-Based
776 Neuromodulation. *Am J Psychiatry* **177**, 435-446 (2020).
777 88. P. B. Fitzgerald *et al.*, A randomized trial of rTMS targeted with MRI based neuro-
778 navigation in treatment-resistant depression. *Neuropsychopharmacology* **34**, 1255-
779 1262 (2009).
780 89. T. Hebel *et al.*, A direct comparison of neuronavigated and non-neuronavigated
781 intermittent theta burst stimulation in the treatment of depression. *Brain Stimul* **14**,
782 335-343 (2021).
783 90. S. H. Kennedy *et al.*, Differences in brain glucose metabolism between responders to
784 CBT and venlafaxine in a 16-week randomized controlled trial. *Am J Psychiatry* **164**,
785 778-788 (2007).
786 91. H. S. Mayberg *et al.*, Reciprocal limbic-cortical function and negative mood: converging
787 PET findings in depression and normal sadness. *Am J Psychiatry* **156**, 675-682 (1999).

92. M. S. Nobler *et al.*, Decreased regional brain metabolism after ect. *Am J Psychiatry* **158**, 305-308 (2001).
93. H. S. Mayberg, Targeted electrode-based modulation of neural circuits for depression. *The Journal of clinical investigation* **119**, 717-725 (2009).
94. J. G. Ojemann *et al.*, Anatomic localization and quantitative analysis of gradient refocused echo-planar fMRI susceptibility artifacts. *Neuroimage* **6**, 156-167 (1997).
95. L. Schmaal *et al.*, Cortical abnormalities in adults and adolescents with major depression based on brain scans from 20 cohorts worldwide in the ENIGMA Major Depressive Disorder Working Group. *Mol Psychiatry* 10.1038/mp.2016.60 (2016).
96. L. Schmaal *et al.*, Subcortical brain alterations in major depressive disorder: findings from the ENIGMA Major Depressive Disorder working group. *Mol Psychiatry* **21**, 806-812 (2016).
97. O. Esteban *et al.*, fMRIPrep: a robust preprocessing pipeline for functional MRI. *Nat Methods* **16**, 111-116 (2019).
98. C. J. Lynch *et al.*, Automated optimization of TMS coil placement for personalized functional network engagement. *Neuron* **110**, 3263-3277.e3264 (2022).

806 **Figure Legends**

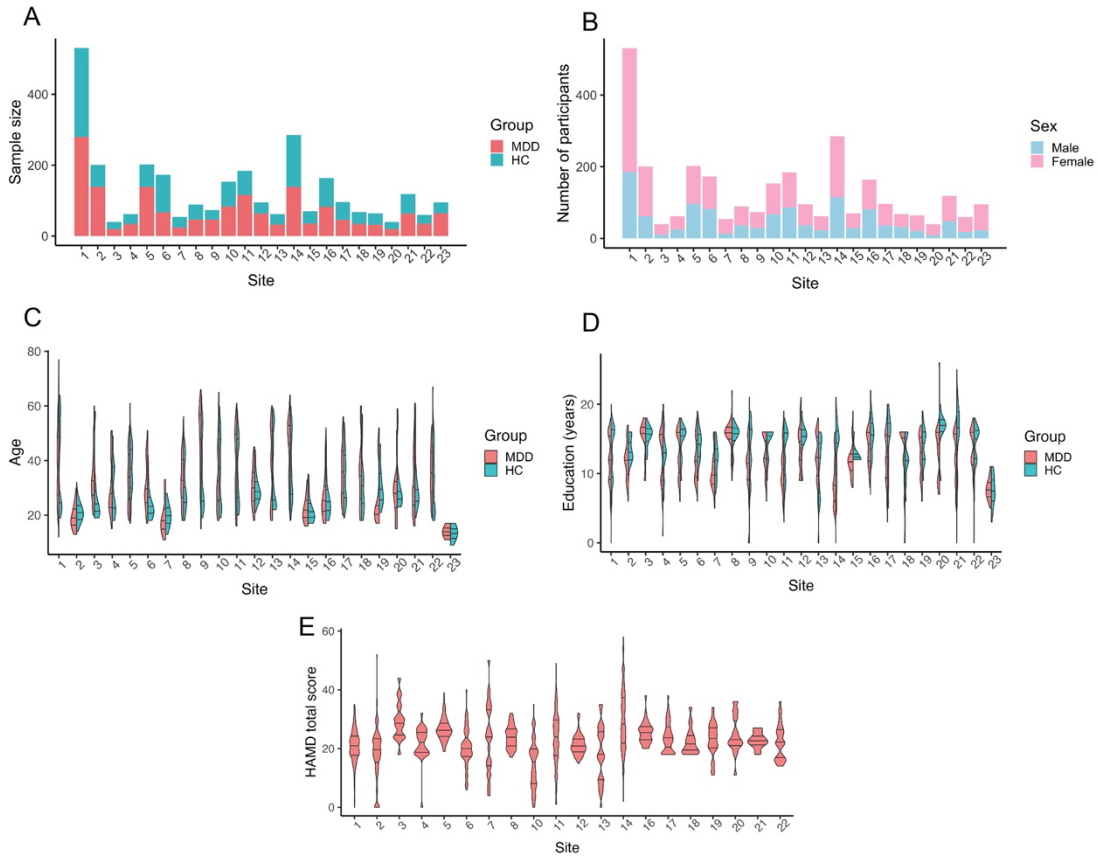

807

808 Figure 1. Depression Imaging REsearch ConsorTium (DIRECT) Phase II sample characteristics.
809 (A) Sample sizes of each site; (B) Number of male/female subjects irrespective of diagnosis; (C)
810 Violin plots depicting the distribution of age (in years). Solid black lines indicate the mean, 25th
811 and 75th percentiles; (D) Violin plots show education distribution (in years). Solid black lines
812 indicate the mean, 25th and 75th percentiles; (E) Violin plots depicting the distribution of scores
813 of the Hamilton Depression Rating Scale (HAMD). Solid black lines indicate the mean, 25th and
814 75th percentiles.

815

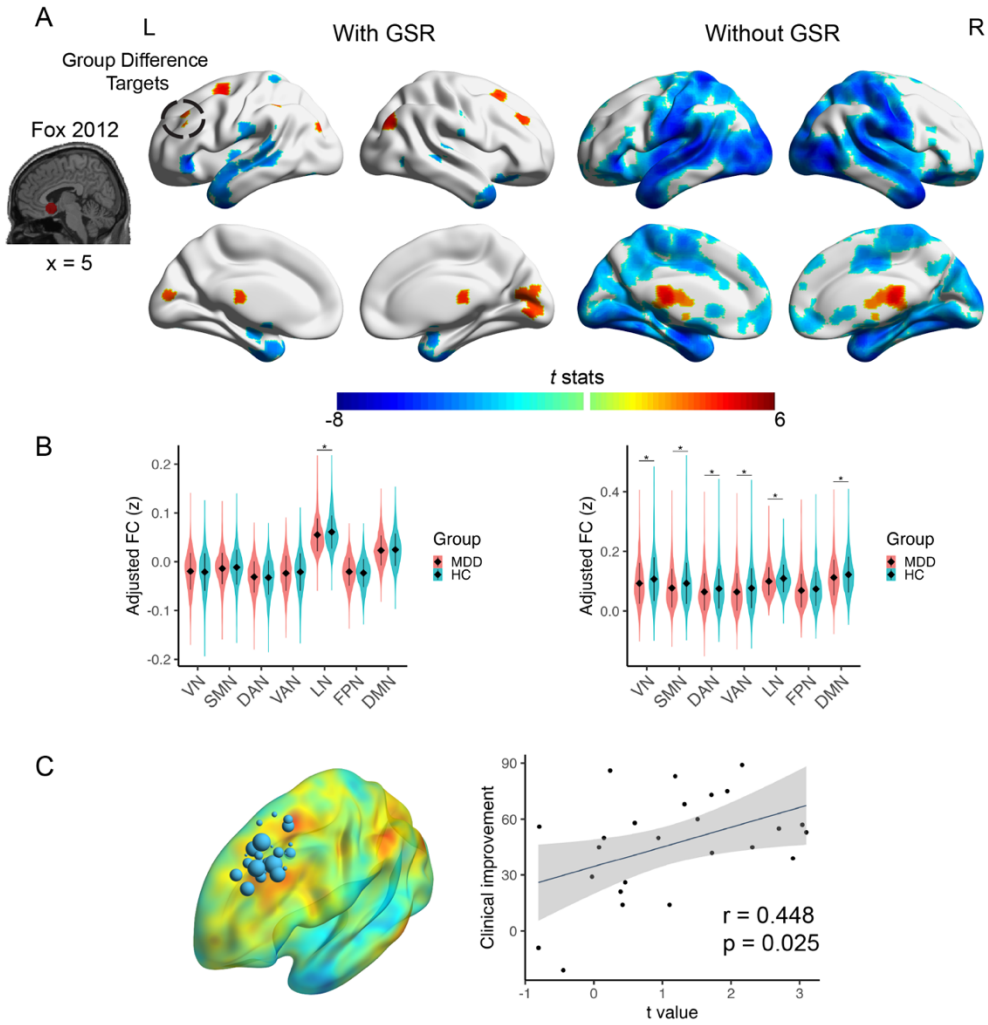

Figure 2. Group difference maps of subgenual anterior cingulate cortex (sgACC) functional connectivity (FC) profiles. (A) t maps of MDD-related sgACC FC abnormalities with and without global signal regression (GSR). (B) Group differences of FCs between sgACC and visual network (VN), somatomotor network (SMN), dorsal attention network (DAN), ventral attention network (VAN), limbic network (LN), frontoparietal network (FPN), and default mode network (DMN). Asterisks indicate significance after Bonferroni correction. (C) The group difference of sgACC FC maps was positively related to clinical improvement following transcranial magnetic stimulation (TMS). Data were extracted from an independent openly shared dataset (33). The sizes of the spheres indicate the reduction rates of the Hamilton Depression Rating Scale (HAMD) and the group difference map after global signal regression (GSR) was rendered on the surface.

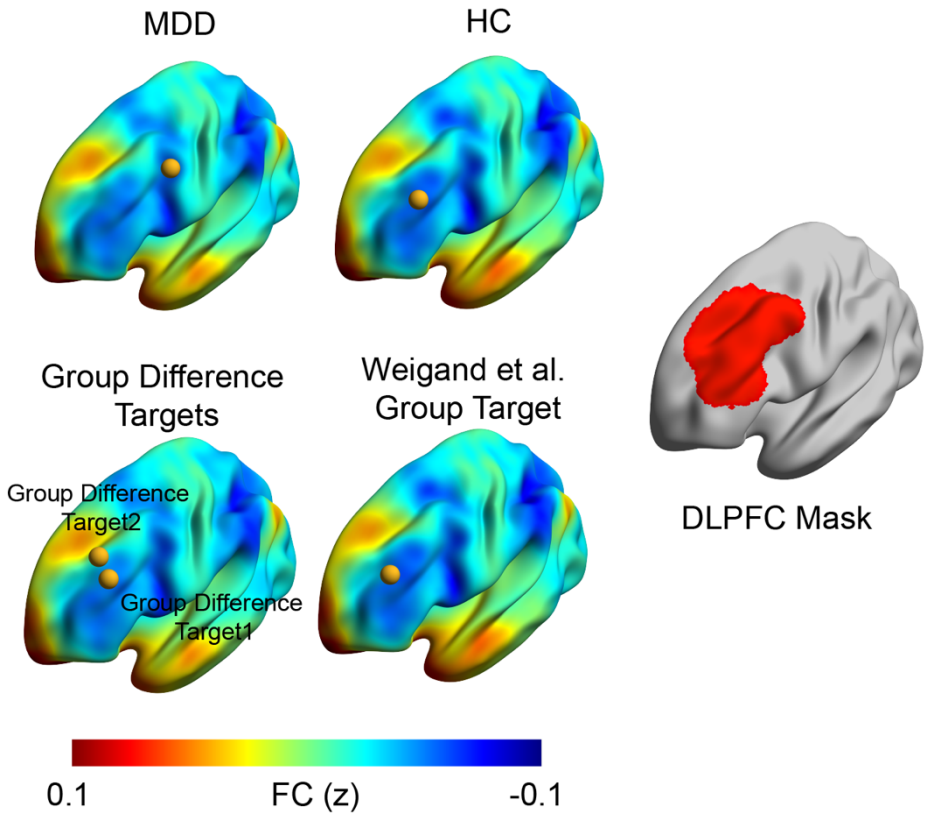

Figure 3. The position of the anti-correlation peak in group mean functional connectivity (FC) differed between major depressive disorder (MDD) patients and healthy controls (HCs). The group mean FC maps of MDD patients (the MDD peak and group difference targets) or HCs (the HC peak and Weigand et al. group target) after GSR were rendered on the surface. The "group difference targets" and a previously reported subgenual anterior cingulate cortex (sgACC) target calculated based on a large cohort of healthy adults (33) were also plotted for illustration. Peaks were searched within the left dorsal lateral prefrontal cortex (DLPFC) mask.

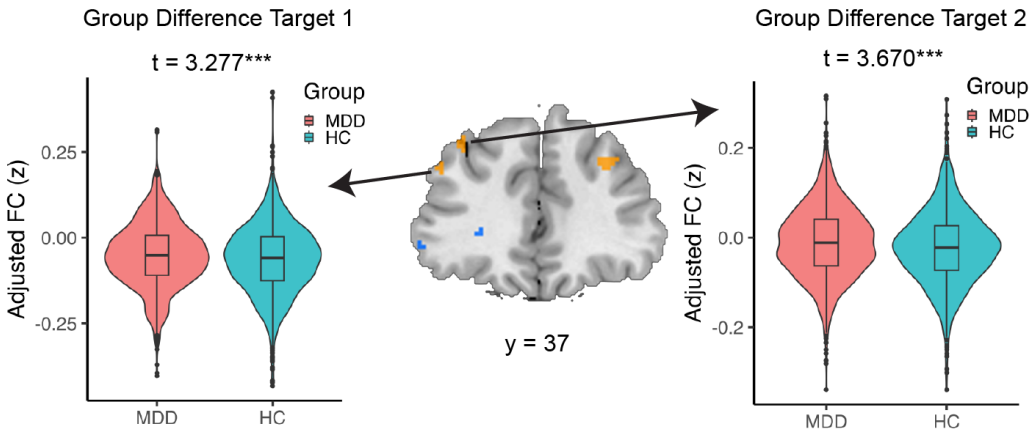

Figure 4. Two clusters showed significant case-control differences in functional connectivity (FC) with the subgenual anterior cingulate cortex (sgACC). The peaks of these two clusters were chosen as “group difference targets.”

844

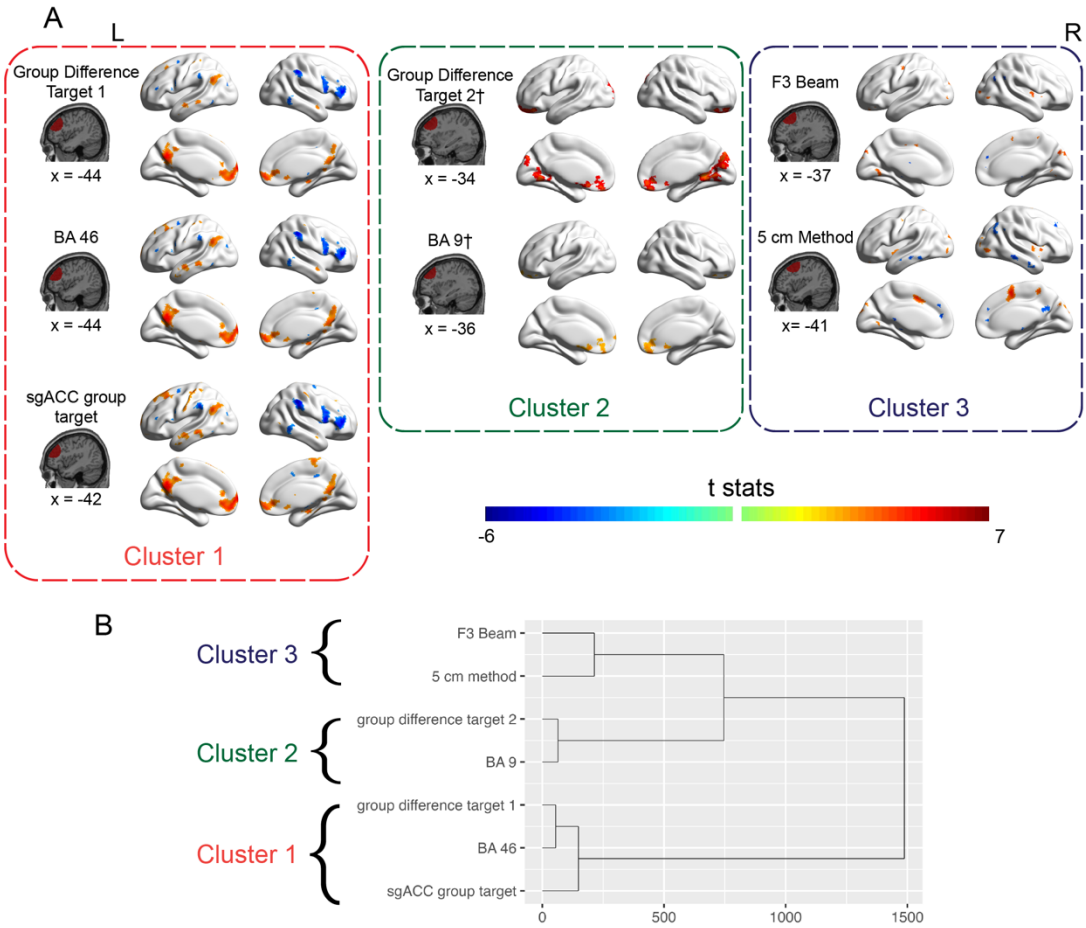

845

846 Figure 5. The group difference maps of different left dorsal lateral prefrontal cortex (DLPFC)
847 regions of interest (ROI) could be grouped into 3 clusters. (A) MDD-related DLPFC FC
848 abnormalities. (B) The hierarchical clustering of left DLPFC ROIs' case-control difference maps.
849 †: Corrected with Gaussian random field correction at the threshold of voxel-wise $p < 0.01$ and
850 cluster-wise $p < 0.05$, two-tailed.

851

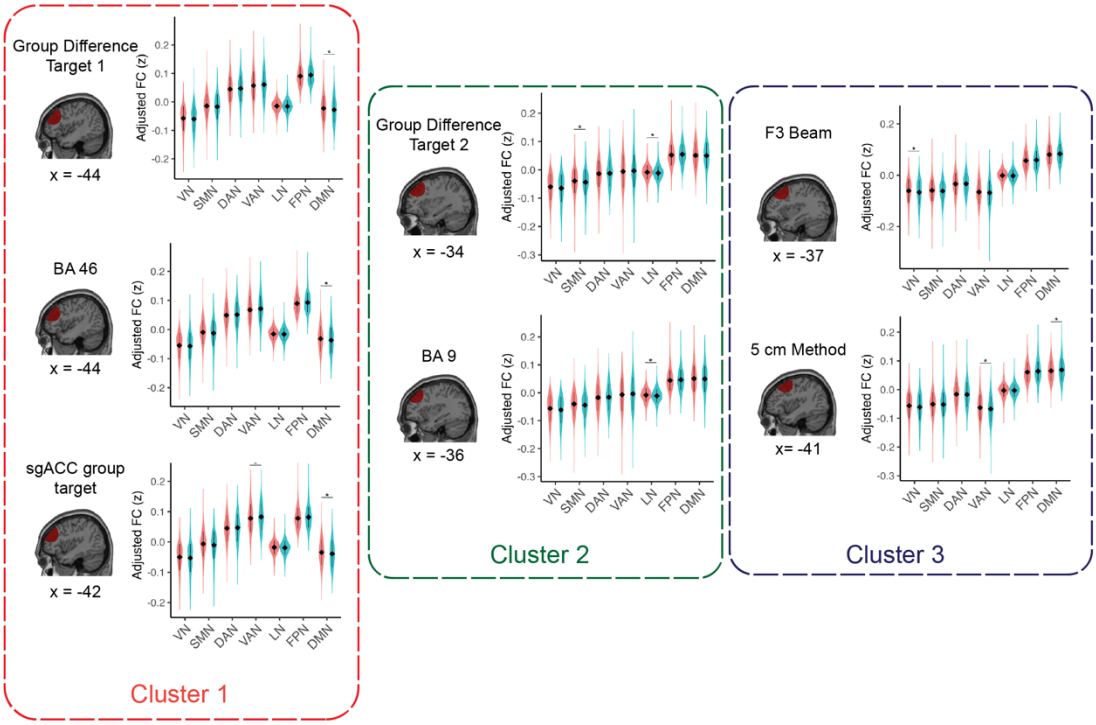

852

853 Figure 6. Group differences of FCs between the different left dorsal lateral prefrontal cortex
854 (DLPFC) regions of interest (ROI) and visual network (VN), somatomotor network (SMN), dorsal
855 attention network (DAN), ventral attention network (VAN), limbic network (LN), frontoparietal
856 network (FPN), and default mode network (DMN). Asterisks indicate significance after
857 Bonferroni correction.